Available online at www.sciencedirect.com

ScienceDirect

Procedia CIRP 14 (2014) 383 – 388

www.elsevier.com/locate/procedia

6th CIRP International Conference on High Performance Cutting, HPC2014

Estimation of cutting conditions in precision micromachining of CuNi alloys of varying composition

Tom Childs[a], Chris Tyler[b], Chris Evans[b,*], Tony Schmitz[b], Ed Paul[b,c], Eric Browy[b]

[a]*School of Mechanical Engineering, University of Leeds, Leeds LS2 9JT, UK;*
[b]*Department of Mechanical Engineering and Engineering Sciences, University of North Carolina-Charlotte, Charlotte NC 28223, USA;*
[c]*Stockton College, Galloway, NJ 08205, USA.*

* Corresponding author. Tel.: +01-704-687-5869; fax: +01-704-687-8345. *E-mail address:* cevans52@uncc.edu

Abstract

A non-dimensional model is developed that relates cutting edge temperatures to process inputs (speed and feed) and outputs (cutting and thrust forces) as well as tool and work thermal properties in micromachining with diamond tools. The temperature estimates are used to determine activation energy for thermally activated chemical wear of a PCD tool milling Monel 400 (Cu 32, Ni 65 wt%). Activation energy estimates are from 15 to 60 kJ / mole, depending on systematic uncertainties, such as diamond thermal conductivity, that still need to be addressed.

Selection and peer-review under responsibility of the International Scientific Committee of the 6th CIRP International Conference on High Performance Cutting

Keywords: Diamond cutting tools, Chemical wear, Temperature modelling

1. Introduction

Precision micromachining is typically carried out with single crystal diamond (SCD) tools, for example nose turning, or polycrystalline diamond (PCD) tools, for example milling [1,2]. The wear of these tools is important for both cut surface quality and cost reasons.

There is much evidence that diamond tool wear is in part of chemical origin. Wear correlates with electronic structure when machining elemental metals [3]. Wear in machining Ni is reduced with increased phosphorous [3] and in machining steels is reduced by nitriding [4]. However the chemical effects are complicated and unclear. For example, diamond wear in steel machining is reduced in a hydrocarbon environment in some conditions [5] but not in others [6].

The question posed in this paper is whether diamond tool chemical wear can be predicted for a range of alloys. The CuNi system is chosen for study as it is both intellectually attractive and practically important. The system is single phase over its whole range, from pure Cu causing negligible chemical wear to pure Ni causing rapid chemical wear.

It is assumed that chemical wear rate is controlled by the Arrhenius equation. It then depends on an activation energy and the temperature of cutting. While activation energy may vary with alloy composition, temperature depends on the mechanics of cutting. Tool temperature is difficult to measure at the scale of micromachining. Forces can be measured. As a first stage of predicting alloy chemical wear rates, this paper develops micromachining models for CuNi alloys that predict tool temperatures from forces. Predictions are presented non-dimensionally so that they can be applied to a range of alloys.

In this paper predictions are applied to milling, estimating temperature and hence activation energy for wear of a PCD tool milling a nominal 65Ni32Cu wt % alloy (Monel 400). Milling with PCD is chosen over nose turning with SCD because the typically larger chip loads enable easier force measurement in milling, and PCD tools are cheaper.

There has recently been other work of similar nature, estimating tool temperatures to obtain activation energy from the wear of SCD tools machining a low carbon steel [7]. Temperatures were estimated for the particular test conditions by finite element analysis. The present paper provides a broader analysis of wider applicability.

Selection and peer-review under responsibility of the International Scientific Committee of the 6th CIRP International Conference on High Performance Cutting
doi:10.1016/j.procir.2014.03.020

2. Theory

Figure 1a shows (hatched) the crescent-shaped uncut cross-section of material machined from a workpiece in one pass by a single flute milling cutter. Figure 1b shows an instant of chip formation when the tool wear area is w. A model for tool edge temperature variation throughout the cutting cycle, and the consequent tool wear, is the subject of this section.

Independent variables are cutting speed $v_c = \pi D\Omega$, (D the cutter diameter, Ω the rotation speed), contact arc s subtending θ at the cutter's centre, and uncut chip thickness h, varying approximately linearly with cut distance 0 to s, from h_{max} to 0 (down milling) or 0 to h_{max} (up milling). By geometry:

$$\theta \approx 2(a_e / D)^{0.5}$$
$$s = (D/2)\theta$$
$$h_{\max} \approx f \sin\theta$$
$$f = v_f / \Omega$$

where a_e is the radial depth of cut, f the feed per tooth and v_f the work feed velocity.

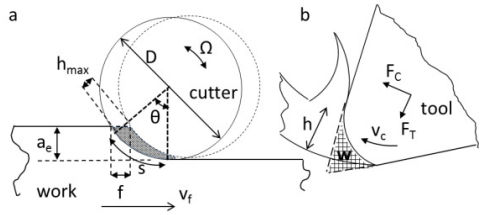

Fig.1. Milling (a) general view, (b) up milling detail.

2.1. Finite element simulations

Simulations have been performed, with commercial code AdvantEdge-2D in custom material mode, to obtain tool edge temperatures for both continuous cutting (h independent of cut distance) and milling (h varying with cut distance). For both, the high conductivity (K_{tool}) of diamond tools with the thin chips of micromachining result in the primary shear heat that flows to the chip being conducted into the tool, instead of being carried away by the chip. The tool's edge becomes its hottest part. Figure 2 illustrates these for continuous cutting. Isotherms between the primary shear zone and tool radiate approximately from the cutting edge. Heat flow is normal to the isotherms, towards the tool. Maximum tool temperature at the tool's edge is clear.

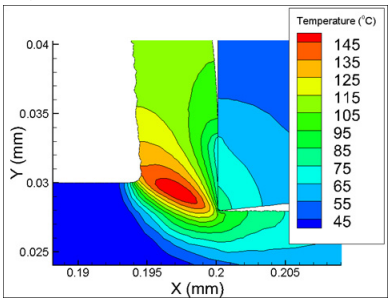

Fig. 2. Continuous chip formation and isotherms for a Monel alloy: h = 2 µm, v_c = 280 m/min, K_{tool} = 500 W/mK. (h = 200 µm, v_c = 2.8 m/min gives the same distribution.)

A classical heat conduction analysis and simulations of continuous cutting, for tools with rake angle γ = 0 (the subject of this work), details to be submitted elsewhere, show the dimensionless group $(K_{tool}\Delta T_{tool})/(F_C{*}hv_c)$ to vary with $[(hv_c)/(4\kappa_{tool})]^{0.5}$and (K_{work}/K_{tool}), with a further approximate dependence on $(F_T{*}/F_C{*})$, where ΔT_{tool} is the tool edge temperature rise, $F_C{*}$ and $F_T{*}$ are specific cutting and thrust forces, K_{tool} and K_{work} are tool, work thermal conductivities and κ_{work} is work thermal diffusivity. Figure 3 summarizes results for hv_c in the range 0.25 to 10 mm^2/s (κ_{work} = 6 mm^2/s). $[(K_{tool}\Delta T_{tool})/(F_C{*}hv_c) + F_T{*}/F_C{*}]$ reduces linearly with increasing $[(hv_c)/(4\kappa_{work})]^{0.5}$. Identical products of h and v_c for example h = 2 µm and v_c =280 m/min or h=20 µm and v_c=28 m/min give the same result (Figure 2 gives an example). K_{work} and K_{tool} are 22 and 500 W/mK respectively). Different values of $F_T{*}/F_C{*}$ (or friction angles λ) are obtained by varying the chip / tool friction coefficient μ input to the simulations and work strain hardening, to give different shear angles ϕ. Fig. 4 compares (λ, ϕ) simulation outputs with values from copper micromachined (h = 1 to 10 µm) with single crystal diamond tools [8,9] and in general engineering conditions (h = 0.1 to 0.2 mm and carbide tools) [10].

The overlap in Figure 4 between the simulated and experimental data supports the simulations' continuous machining validity. From the narrow spread of data in Fig. 3 ΔT_{tool} may be estimated to within ± 10 to 20% if h, v_c, K_{tool}, κ_{work}, $F_C{*}$ and $F_T{*}$ are known.

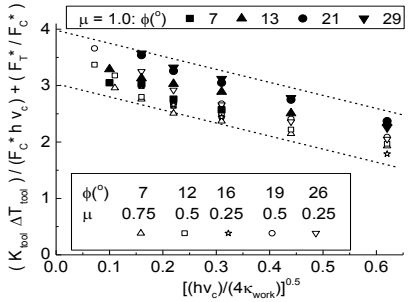

Fig. 3. Dependence of $(K_{tool}\Delta T_{tool})/(F_C{*}hv_c) + (F_T{*}/F_C{*})$ on $[(hv_c)/(4\kappa_{tool})]^{0.5}$ from continuous cutting simulations. (μ,ϕ) indicate different chip formation conditions.

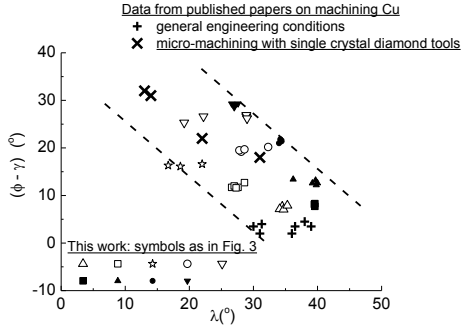

Fig. 4. Previous experimental [8-10] and simulated (ϕ, λ) data compared.

Simulations with tool conductivity between 200 and 2000 W/mK and 3D simulations for the effect of aspect ratio w_c/h on ΔT_{tool}, with w_c the width (a_p) of the chip, have also been

carried out. The combination of results gives, for $[(hv_c)/(4\kappa_{work})]^{0.5} < 0.6$ and $K_{work}/K_{tool} < 0.1$

$$\frac{K_{tool}\Delta T_{tool}}{F_C^* h v_c} = \left(0.38 + 0.14\ln\frac{w_c}{h}\right)\left(1.2 - 3.8\frac{K_{work}}{K_{tool}}\right) \text{x}\left[3.5 \pm 0.5 - \frac{F_T^*}{F_C^*} - 2.3\left(\frac{hv_c}{4\kappa_{work}}\right)^{0.5}\right] \quad (1)$$

The detail of this paper extends this to the unsteady conditions of milling (h varying with cut distance). A milling cutter removing a crescent-shaped cross-section from work (Figure 1) is approximated by a tool cutting into a surface of constant slope h_{max}/s. Figure 5 shows for up milling (left) and down milling (right) an example of geometry (top, with the y-scale twice the x-scale), chip form at mid-cut (middle) and force and temperature variations (bottom). The particular conditions are given in the caption.

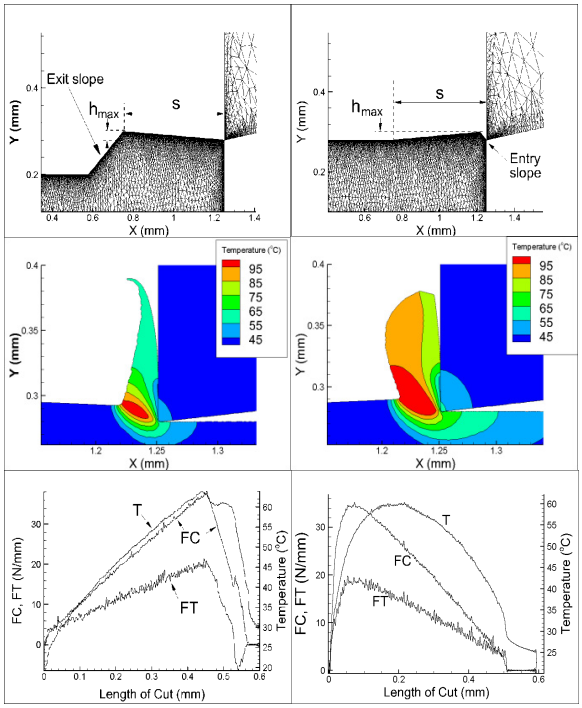

Fig. 5. Typical up milling (left) and down milling (right) simulation geometry and results. In this case h_{max} = 20 µm, s = 0.5 mm, v_c = 28 m/min, material inputs as for (µ,ϕ) (Figure 3) = (0.5, 19°)

Variations of ΔT_{tool}, F_C and F_T with cut distance, and thus h, are extracted and $(K_{tool}\Delta T_{tool})/(F_C^* h v_c) + F_T^*/F_C^*$ obtained. Figure 6 shows the dependencies on $[(hv_c)/(4\kappa_{tool})]^{0.5}$ for the same example as Figure 5, compared with that for continuous cutting. Up milling results follow those from continuous cutting, but displaced to lower values. Down milling results vary more with $[(hv_c)/(4\kappa_{tool})]^{0.5}$. Figure 7 gives more detailed examples. In both down (Figure 7a) and up (Figure 7b) milling, increasing the slope h_{max}/s displaces results towards the origin without change of slope. The product $(h_{max}v_c)$ hardly displaces the results (Figure 7a) nor does the chip formation as defined by (μ,ϕ) (Figure 7b), as in continuous cutting.

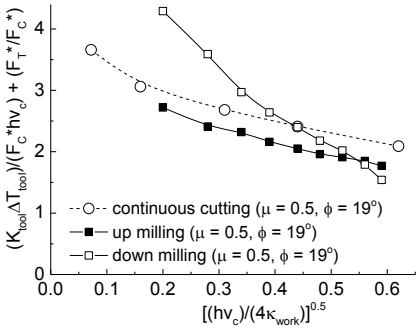

Fig. 6. $[(K_{tool}\Delta T_{tool})/(F_C^* h v_c) + F_T^*/F_C^*]$ v. $[(hv_c/4\kappa_{work})]^{0.5}$ compared for continuous cutting and milling.

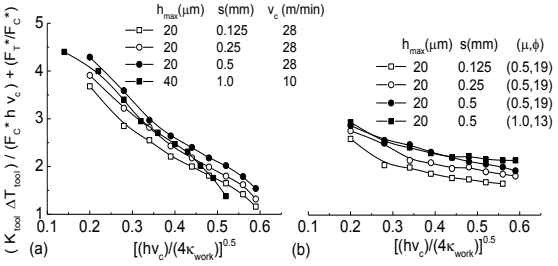

Fig. 7. Influences, in the manner of Figure 6, of h_{max}/s in (a) down and (b) up milling; also (a) of (h_{max}, v_c) and (b) (μ,ϕ) friction and material combination.

The influence of h_{max}/s on ΔT_{tool} in up milling (Figure 7b) is described by extending Equation (1) to

$$\frac{K_{tool}\Delta T_{tool}}{F_C^* h v_c} = \left(0.38 + 0.14\ln\frac{w_c}{h}\right)\left(1.2 - 3.8\frac{K_{work}}{K_{tool}}\right) x\left[3.5 \pm 0.5 - \frac{F_T^*}{F_C^*} - 2.3\left(\frac{h_{max}}{s}\right)^{0.57} - 2.3\left(\frac{hv_c}{4\kappa_{work}}\right)^{0.5}\right] \quad (2)$$

2.2. Thermally activated wear analysis

When edge wear w (Figure 1b) is thermally activated, the wear increment in one pass of a cutting edge (time t = 0 to s/v_c) is given by Equation (3), with E activation energy, R the gas constant T_0 ambient absolute temperature and A^* a rate constant:

$$\Delta w = A^* \int_0^{s/v_c} \exp\left[-\left(E/\mathrm{R}\right)/\left(T_0 + \Delta T_{tool}(t)\right)\right] dt \quad (3)$$

With respect to cut distance x ($x = v_c t$), Equation (3) becomes

$$\Delta w = \left(A^*/v_c\right) \int_0^{s} \exp\left[-\left(E/\mathrm{R}\right)/\left(T_0 + \Delta T_{tool}(x)\right)\right] dx \quad (4)$$

The work area ΔA removed by one chip is fa_e, and v_c is proportional to Ω (Figure 1). If two milling operations 1 and 2 are undertaken with the same f, a_e but different Ω,

$$\frac{(dw/dA)_1\,\Omega_1}{(dw/dA)_2\,\Omega_2} = \frac{\left(\int_0^s \exp\left[-(E/\mathrm{R})/(T_0+\Delta T_{tool}(x))\right]dx\right)_1}{\left(\int_0^s \exp\left[-(E/\mathrm{R})/(T_0+\Delta T_{tool}(x))\right]dx\right)_2} \quad (5)$$

If dw/dA, the wear area per cut area, is measured in a pair of tests keeping f, a_e constant, varying v_c and therefore the tool temperature, E can be found by solving Equation (5) numerically. For more than one pair, an optimum E can be determined.

3. Experiments

Up milling has been carried out with a zero axial and radial rake angle single flute PCD tool (assumed K_{tool} 500 W/mK), D = 3.175 mm, f = 0.08 mm/tooth, a_e = 0.1D mm, Ω = 1000 and 375 RPM. Then (Figure 1), θ = 0.63 rads, s = 1.0 mm, h_{max} = 50 µm, v_c = 10 and 3.75 m/min. Work material is Monel 400 (assumed K_{work} 22 W/mK, κ_{work} 6 mm^2/s). These give $[(h_{max}v_c)/(4\kappa_{tool})]^{0.5}$ = 0.59 and 0.36 and h_{max}/s = 0.05. Figure 8 is an image of an unworn tool. From a larger magnification view the cutting edge radius is estimated to be ≈ 2.5 µm.

Figure 9 is a schematic view of the milling set-up. The Monel work is mounted on a Kistler force table. The milling tool removes a 0.5 mm thick, 50 mm long, pre-prepared fin from the work in 10 passes before the fin needs re-machining. Forces F_x and F_y are measured. After testing, the tool is removed for SEM examination.

Initial tests were carried out dry but the main program applies an oil mist atmosphere.

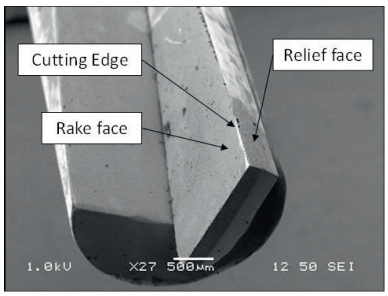

Fig. 8. An unworn tool.

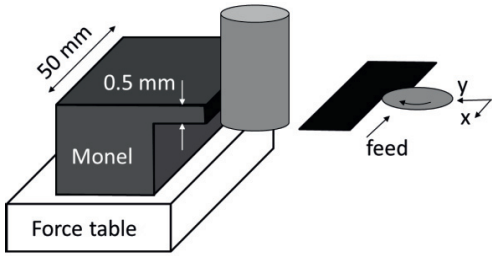

Fig. 9. Schematic (not to scale) view of up milling set up, x,y the direction of forces on the tool.

4. Results

Figure 10a shows forces from a test at Ω = 1000 RPM, with no oil mist. The equality of force cycles from one to the next established the test's stability. Poor surface finish resulted. Figure 10b shows forces from a subsequent test with oil mist, also at 1000 RPM. Forces are considerably reduced.

The evolution of peak total force $(F_x^2+F_y^2)^{0.5}$ with cut volume V is shown in Figure 11 for trials at both Ω = 375 (a) and 1000 (b) RPM. Data points are at the end of each pass. After initial periods (V < 30 to 40 mm^3) of rapid changes in force, forces increase more steadily with time. A linear regression gives dF/dV = 0.114 N/mm^3 in the case of (a). In the case of (b) there is a step at V = 80 mm^3. It corresponds to completion of the first 10 passes and starting the next 10. Linear regression before and after the step gives dF/dV = 0.062 ± 0.003 N/mm^3.

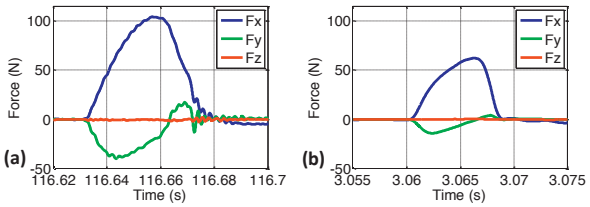

Fig. 10. Forces (F_x > 0), F_y < 0) in up milling: Ω = 1000 RPM, f = 0.08 mm/tooth, a_e = 0.32 mm, axial depth of cut 0.5 mm, (a) dry, (b) with oil mist after 10 passes

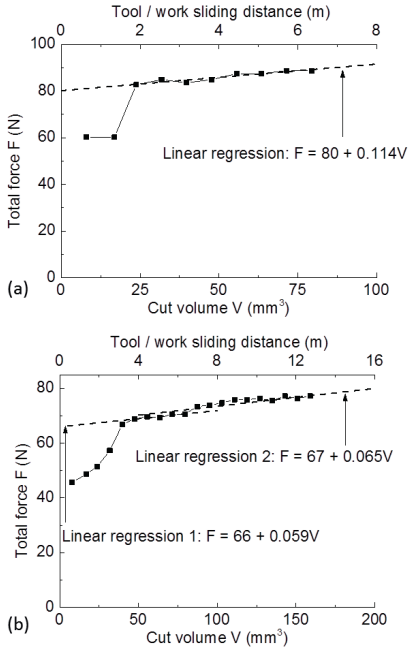

Fig. 11. Force versus cut volume, also versus sliding distance between tool flank and work (a sliding distance s = 1mm occurs with every chip of volume 0.013 mm^3): Ω = (a) 375, (b) 1000 RPM.

Figure 12 shows the worn cutting edge after the test at Ω = 375 RPM. The edge after cutting at 1000 RPM is similar. The extent of the damage is found to be developed after the initial

periods of cutting (V < 30 to 40 mm^3). Figs. 11 and 12 together are consistent with an initial rapid edge breakdown followed by a period of slower wear.

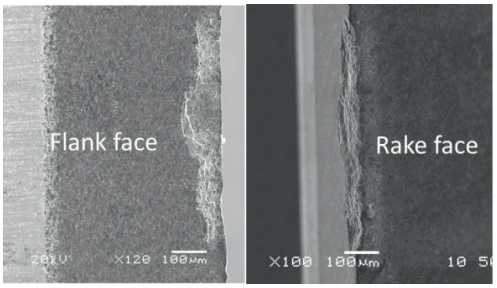

Fig. 12. End of test cutting edge, Ω = 375 RPM.

5. Calculations and further simulations

The measured F_x, F_y over a cut cycle (Figure 10b) can be resolved to F_C, F_T components. Figure 13 shows the variation of F_C with cut distance over one cycle obtained from Figure 10b.

Further up milling simulations have been carried out, in the manner of Figure 5 but for the specific cases h_{max} = 50 µm, s = 1 mm, v_c = 3.75 and 10 m/min (Ω = 375 and 1000 RPM). The predicted F_C for Ω = 1000 RPM is also shown in Figure 13. There is agreement with experiment except near to exit where burr formation is clearly different in practice from that predicted by the simulation.

Figure 13 also includes the cutting edge temperatures predicted by the simulations and from Equation (2). The mean value coefficient 3.5 within Equation (2)'s square bracket is used and the experimental values F_C* = 3.3GPa, F_T* = 2.7 GPa. The coincidence of the simulation and Equation (2) predictions show Equation (2)'s broad applicability.

The right hand side of Equation (5) is evaluated for a range of E with the Equation (2) temperature values from Figure 13. Condition 1 is taken to be Ω = 1000 RPM and 2 to be 375 RPM. It is also evaluated for the upper and lower temperature estimates, replacing the 3.5 in Equation (2) by 4.0 and 3.0 respectively. Figure 14 includes the results.

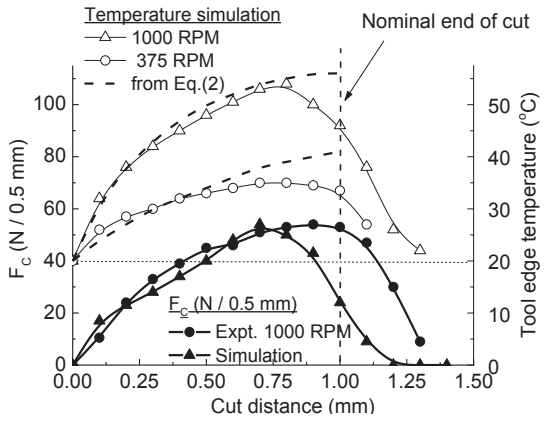

Fig. 13. Experimental and simulated results: F_C (solid symbols with left hand axis) and tool edge temperature (open symbols and dashed lines with right hand axis).

If the steady rate of increase of force with cut volume (Figure 11) is a result of wear, dF/dV may be a proxy for wear rate dw/dV (or dw/dA, Equation (5)). Assuming this, from the values of dF/dV (Figure 11) and Ω_1, Ω_2, the left hand side of Equation (5) = 1.45 in the present case. Figure 14 shows that E = 15, 23 and 45 kJ/mole are estimated from the upper, mid and lower estimates of temperature.

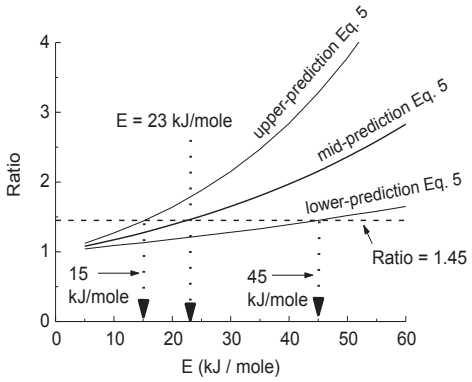

Fig. 14. Dependence of right hand side of Equation (5) (called Ratio) on E, for three temperature estimates, compared to expected value from left hand side of Equation (5).

6. Discussion

Equation (1) and, with the addition of the h_{max}/s term in the case of up milling, Equation (2) are models for the prediction of ΔT_{tool} from measured specific forces F_C*, F_T*, process variables h, v_c and w_c/h, and the tool and work thermal properties K_{tool}, K_{work} and κ_{work}. The simulations on which it is based are validated mechanically through predicting (ϕ, λ) combinations in agreement with experiments (Figure 4) and cutting forces in up milling (Figure 13). They are not validated for their temperature predictions. Further work is needed here.

Even if validated, the uncertainty in Eqs. (1,2) from the coefficient 3.5 ± 0.5 limits the certainty of predicting E by its use (Figure 14). This uncertainty is not a random or computational uncertainty. It is a systematic uncertainty that comes from incomplete knowledge of the strain hardening and friction properties to be applied to the simulations and that affect the chip formation mechanics. It is manifested through the scatter of results in Figure 4. It could be reduced with better knowledge in this area.

In practice, systematic uncertainty also arises through the proportionality between ΔT_{tool} and K_{tool}. Tools are specified by hardness and toughness, not conductivity. True values of conductivity are hard to obtain. It is also unclear whether the values of F_C* and F_T* to be entered into Eqs. (1,2) should be the unworn or the worn tool values. The forces from Figure 10b which agree with the simulated forces in Figure 13 are for a worn tool whereas the simulations neglect wear. If forces were to be reduced to the unworn state, say by 20% (Figure 11), the consequent temperature reduction and re-estimation of E in the manner of Figure 14 leads to E from 18 to 60 kJ/mole with a mid-value of 27 kJ/mole, i.e. an increase of 20 to 30% in the estimates.

The E estimates also assume that observed dF/dV are proportional to dw/dV (or dw/dA). It implies that the tests at both speeds are identical mechanically, their only difference being in their temperatures. That may be so in this case. Figure 12's dF/dV values have been directly used to estimate E. From a tribological view they could have been converted to rates of change with sliding distance dF/ds_d (dV/ds_d = 0.013 mm^2) or to dF/dt (dV/dt = 2.1x10^{-4} Ω mm^3/s). Then, if wear and force change are synonymous, dF/ds_d reducing from 1.5 to 0.81 N/m with increasing Ω (or v_c), i.e. temperature, is not as expected from adhesive or abrasive wear. dF/dt increasing from 9.0 to 13 mN/s with increasing Ω (or v_c) is as expected by a thermally activated wear. Extension of this work to milling a range of CuNi alloys could be expected to show increasing wear with increasing Ni content.

That is the observation in preliminary studies of nose turning (facing) with SCD tools. Figure 15 shows increasing tool wear as Cu content decreases from 90 to 70 to ≈ 30 (Monel 400) wt %. However to convert such observations quantitatively to E values with sufficient certainty to underpin discussion of the particular chemical processes causing the wear will require more certain estimates of temperature than have currently been achieved.

7. Conclusions

Non-dimensional models have been developed from finite element simulations to predict cutting tool edge temperature rise in turning (Equation 1) and up milling (Equation 2) from measured cutting and thrust specific forces, tool and work thermal conductivities, work thermal diffusivity, uncut chip thickness, cutting speed, chip / tool contact aspect ratio and, for milling, the ratio of maximum uncut chip thickness to arc of contact length between cutter and work. The ranges of validity of the equations are $[(hv_c)/(4\kappa_{work})]^{0.5} < 0.6$ and $K_{work}/K_{tool} < 0.1$. These are the typical ranges for micromachining CuNi (and indeed other) alloys machined by either single crystal or polycrystalline diamond tools.

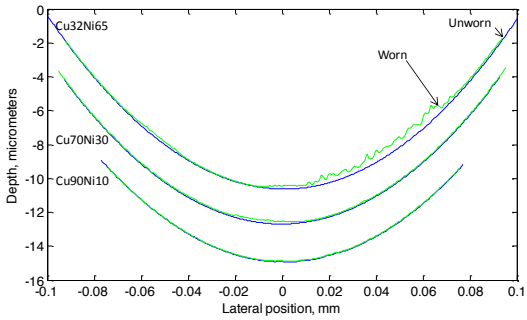

Fig. 15 Edge wear profiles of SCD tools after nose turning (facing at 1000 RPM from 40 to 20 mm diameter) three different CuNi alloys: nose radius 0.5 mm, depth of cut 5 µm, feed 2 µm / rev, total cut distance 1.8 km at an average surface speed of 1.7 m/s [11].

Up milling experiments with polycrystalline diamond tools have been carried out on a Monel 400 alloy at two different cutting speeds. Force increases with cut volume (and time) and tool edge wear have been observed. There is good agreement between the experimental and simulated cutting forces. Assuming that the rates of change of force with time are in proportion to the tool wear rate and that the wear is chemical in origin, and applying the temperatures predicted from the simulations, an activation energy is predicted for the wear in the range 15 to 60 kJ/mole.

The range arises from several causes. Eqs. 1 and 2 have an uncertainty in them due to imperfect knowledge of the chip formation mechanics in micromachining the CuNi alloy with diamond tools; also it is not certain whether the specific forces to be entered in the equations should be those from the sharp or worn tools. In addition the equations predict that the tool edge temperature rise is in direct proportion to the tool thermal conductivity. This has been taken to be 500 W/mK, a commonly assumed value for polycrystalline diamond tools but one which has not been measured for the particular tools employed. Further work is in progress to reduce these systematic uncertainties and to extend the experimental cutting studies to other CuNi alloys.

Acknowledgements

This work was supported in part by NSF Grant 1162209.

References

[1] Dornfeld D, Min S, Takeuchi Y. Recent advances in mechanical micromachining. Annals CIRP 2006;55/2:745-768.

[2] Rhorer, R, Evans CJ. Fabrication of optics by diamond turning. In *Handbook of optics (volume 2) 3rd edition*. New York: McGraw-Hill 2010, Ch.10.

[3] Paul E, Evans CJ, Mangamelli A, McGlauffin ML, Polvani RS. Chemical aspects of tool wear in single point turning. *Precision Engineering* 1996;18:4-19.

[4] Brinksmeier E, Glabe R, Osmer J. Ultra-precision diamond cutting of steel molds. *Annals CIRP* 2006;55/1:551-554.

[5] Casstevens JM. Diamond turning of steel in carbon-saturated environments. *Precision Engineering* 1983;5:9-15.

[6] Hitchiner MP, Wilks J. Some remarks on the chemical wear of diamond and cubic BN during turning and grinding. *Wear* 1987;114:327-338.

[7] Lane BM, Dow TA, Scattergood R. Thermo-mechanical wear model and worn tool shapes for single-crystal diamond tools cutting steel. *Wear* 2013;**300**:216-224.

[8] Moriwaki T, Okuda K. Machinability of copper in ultra-precision micro diamond cutting. *Annals CIRP* 1989;**38/1**:115-118.

[9] Lucca DA, Rhorer RL, Komanduri R. Energy dissipation in the ultraprecison machining of copper. *Annals CIRP* 1991;**40/1**:69-72.

[10] Childs THC, Maekawa K, Obikawa T, Yamane Y. *Metal machining: Theory and applications*, London: Arnold; 2000, p. 85-89.

[11] in preparation for *Optical Fabrication and Testing Workshop,* Optical Society of America: Hawaii, 22-26 June, 2014.